Available online at www.sciencedirect.com
SCIENCE DIRECT®
Journal of Solid State Chemistry 177 (2004) 3359–3367
JOURNAL OF SOLID STATE CHEMISTRY
http://elsevier.com/locate/jssc

Crystal chemistry and crystallography of the Aurivillius phase $Bi_5AgNb_4O_{18}$

W. Wong-Ng,[a,*] Q. Huang,[a] L.P. Cook,[a] I. Levin,[a] J.A. Kaduk,[b] A.D. Mighell,[a] and J. Suh[a]

[a] *Materials Science and Engineering Laboratory, National Institute of Standards and Technology, Materials Bldg., Rm A-207, Gaithersburg, MD 20899, USA*

[b] *British Petroleum Chemicals, P.O. Box 3011 MC F-9, Naperville, IL 60566, USA*

Received 20 November 2003; received in revised form 18 May 2004; accepted 20 May 2004

Available online 20 July 2004

Abstract

$Bi_5AgNb_4O_{18}$ is a new phase, which was discovered during the phase equilibrium study of the Bi_2O_3–Ag_2O–Nb_2O_5 system. $Bi_5AgNb_4O_{18}$ was prepared at 750°C and is stable in air up to its melting temperature of 1160.1 ± 5.0°C (standard error of estimate). Results of a Rietveld refinement using neutron powder diffraction confirmed that $Bi_5AgNb_4O_{18}$ is isostructural with Bi_3TiNbO_9, $Bi_5NaNb_4O_{18}$, and $Bi_5KNb_4O_{18}$. The structure was refined in the orthorhombic space group $A2_1am$, $Z = 2$, and the lattice parameters are $a = 5.4915(2)$ Å, $b = 5.4752(2)$ Å, $c = 24.9282(8)$ Å, and $V = 749.52(4)$ Å^3. The structure can be described as the $m = 2$ member of the Aurivillius family, $(Bi_2O_2)^{2+}$ $(A_{m-1}B_mO_{3m+1})^{2-}$ (where A =Bi and B = Ag, Nb), which is characterized by perovskite-like $(A_{m-1}B_mO_{3m+1})^{2-}$ slabs regularly interleaved with $(Bi_2O_2)^{2+}$ layers. The octahedral $[NbO_6]$ units are distorted with Nb–O distances ranging from 1.856(4) to 2.161(2) Å and the O–Nb–O angles ranging from 82.6(3)° to 98.5(3)°. These octahedra are tilted about the a- and c-axis by about 10.3° and 12.4°, respectively. Ag was found to substitute exclusively into the Bi-site that is located in the layer between the two distorted $[NbO_6]$ units. Although the Ag substitutes into the Bi-site with the Bi:Ag ratio of 1:1, the existence of a superlattice was not detected using electron diffraction. A comparison of $(Bi_2O_2)^{2+}(A_{m-1}Nb_mO_{3m+1})^{2-}$ structures (where A =Ag, Na, and K) revealed a relation between the pervoskite tolerance factor, t, and structural distortion. The reference pattern for $Bi_5AgNb_4O_{18}$ has been submitted to the International Centre for Diffraction Data (ICDD) for inclusion in the Powder Diffraction File.

Published by Elsevier Inc.

Keywords: Aurivillius phase; Structure of $Bi_5AgNb_4O_{18}$; Neutron and X-ray Rietveld refinements; X-ray reference diffraction pattern; Structure comparison of $Bi_5ANb_4O_{18}$ (A = K, Ag, Na)

1. Introduction

Low-temperature cofired ceramics (LTCC) technology has demonstrated many advantages, and has become important for various electronics device applications. Since the first wide-spread application of LTCC in ceramics packaging more than a decade ago [1], the increased use of LTCC to incorporate an array of embedded electronics components [2] in recent years has led to intensive research in this important area of ceramics.

Compositions in the Bi_2O_3–Nb_2O_5 system have been shown to be important for LTCC technology [3,4]. To minimize conductor losses, the choice of the appropriate electrode is limited. Ag is the metallization of choice in many LTCC fabrications because of its outstanding electrical conductivity and low cost relative to other noble metals [5,6]. Since it is important to understand the reactions between phases of the Bi_2O_3–Nb_2O_5 system [7,8] with Ag, a systematic study of the phase diagram of the Bi_2O_3–Ag_2O–Nb_2O_5 system has been conducted [9]. In the course of this investigation, a phase with chemical formula $Bi_5AgNb_4O_{18}$ was identified. Although $Bi_5AgNb_4O_{18}$ was briefly reported by Valant et al. [6], no structural data are available. As crystal

*Corresponding author. Fax: +1-301-975-5334.
E-mail address: winnie.wong-ng@nist.gov (W. Wong-Ng).

0022-4596/$ - see front matter Published by Elsevier Inc.
doi:10.1016/j.jssc.2004.05.040

structure affects physical properties significantly, the main goal of this study is to understand the crystal chemistry and crystallography of $Bi_5AgNb_4O_{18}$ using X-ray, neutron and electron diffraction techniques, and differential thermal analysis/thermal gravimetric analysis (DTA/TGA).

The powder X-ray diffraction technique is of primary importance for phase characterization, therefore extensive coverage and accurate reference diffraction patterns of the perovskite-related phases in the Powder Diffraction File (PDF)[1] are essential for materials research community. Currently, the powder pattern of $Bi_5AgNb_4O_{18}$ is not in the PDF, therefore the second goal of this investigation is to determine reference diffraction patterns for $Bi_5AgNb_4O_{18}$ using the X-ray Rietveld refinements technique [10–12].

2. Experimental[2]

The sample $Bi_5AgNb_4O_{18}$ was prepared using the solid-state sintering technique. A stoichiometric amount of 5:1:4 ratio of Bi_2O_3, Ag_2O, and Nb_2O_5 was homogenized using a mortar and pestle. Well-mixed stoichiometric compacted powder was prepared by pressing the powder in a pelletizing die to about 0.3 GPa. The compacted powder was heated in air at 500°C for 2 days followed by 700°C for 1 day and 750°C for 1 week. Each time after the samples were taken out of the furnace, they were reground and repelletized. Synthesis was carried out with the reagents weighted as needed to yield an approximately 8 g sample for both neutron diffraction study and X-ray diffraction pattern preparation.

X-ray powder diffraction was used to identify the phases synthesized and to confirm phase purity. A computer-controlled automated diffractometer equipped with a θ-compensation slit and Cu$K\alpha$ radiation was operated at 45 kV and 40 mA. The radiation was detected by a scintillation counter and solid-state amplifier. The Siemens software package and the reference X-ray diffraction patterns of the PDF were used for performing phase identification.

Following the initial X-ray diffraction work, the compound was subsequently studied via neutron powder diffraction. Neutron diffraction data were collected with the 32 detector BT-1 diffractometer at the NBSR research reactor of the National Institute of Standards and Technology using a Cu (311) monochromator ($\lambda = 1.5396(1)$ Å). Samples were loaded in a 6 mm diameter vanadium container. Measurements were made under ambient conditions.

The structural refinement was performed by using the GSAS software suite [10–12]. The initial model used was Bi_3TiNbO_9 [13]. The neutron scattering length of the elements Nb/Ag/Bi are 0.71/0.6/0.86, respectively. The parameters refined included scale factor, background function (high order polynominals), profile parameters U, V, W, asymmetry coefficient, lattice parameters, atomic coordinates, and isotropic temperature factors.

Specimens for transmission electron microscopy (TEM) were prepared by dispersing powder that had been crushed in ethanol onto lacey-carbon-coated copper grids. The specimens were examined in a transmission electron microscope Philips EM430 operated at 200 kV. The specimens exhibited poor quality due to a lack of cleavage for the $Bi_5AgNb_4O_{18}$ particles upon crushing.

Reference X-ray pattern of $Bi_5AgNb_4O_{18}$ was obtained with a Rietveld pattern decomposition technique. These patterns represent ideal specimen patterns. They are corrected for systematic errors both in d-spacing and intensity. The reported peak positions are calculated from the refined lattice parameters, as this represents the best measure of the true positions.

Fully crystallized $Bi_5AgNb_4O_{18}$ was investigated by DTA/TGA up to 1100°C. A. Mettler TA1 Thermoanalyzer outfitted with an Anatech digital control and data-acquisition system was used. The apparatus was calibrated against the α/β quartz transition (571°C) and the melting points of NaCl (801°C) and Au (1064°C). MgO crucibles were used to contain the sample; separate experiments established that, while magnesium niobates are potential reaction products, in the absence of melt, no reaction occurs between MgO crucibles and Bi–Ag–Nb–O materials up to $\approx$1400°C. Further, the use of MgO containers was found not to affect the temperatures of initial melting below 1400°C. During the DTA/TGA experiments, temperature was ramped at 10°C/min, and purified (CO_2- and H_2O-scrubbed) air was flowed continuously through the sample area.

3. Results and discussion

$Bi_5AgNb_4O_{18}$ was confirmed to be isostructural with Bi_3TiNbO_9, $Bi_5NaNb_4O_{18}$, and $Bi_5KNb_4O_{18}$ [14]. Result of the DTA/TGA experiment shows that there is only one event (endothermic) which takes place at around 1160.1 ± 5.0°C (standard error of estimate). This event corresponds to the melting of $Bi_5AgNb_4O_{18}$ in air. No lower temperature phase transformations were observed.

[1] PDF produced by ICDD, Newtown Square, 12 Campus Blvd., Newtown Squares, PA 19073-3273, USA.

[2] Certain trade names and company products are mentioned in the text or identified in illustrations in order to adequately specify the experimental procedure and equipment used. In no case does such identification imply recommendation or endorsement by National Institute of Standards and Technology.

3.1. Crystal structure determination of $Bi_5AgNb_4O_{18}$

Fig. 1 gives an indexed X-ray powder diffraction pattern for $Bi_5AgNb_4O_{18}$. Selected $h\,k\,l$ values are indicated. All peaks of the pattern are indexable assuming an orthorhombic cell and space group ($A2_1am$) cell [15]. No detectable impurity phase was observed. The lattice of this structural type has been customarily described as A-centered even though it belongs to a non-standard setting so that the direction of polarization is along the a-axis [14]. The neutron Rietveld least-squares refinement method gives the final A-centered unit-cell parameters to be ($a = 5.4915(2)$ Å, $b = 5.4752(2)$ Å, $c = 24.9282(8)$ Å, and $V = 749.52(4)$ Å^3, $Z = 2$, density = 8.031 gm/cm^3).

The final neutron refinement residuals for $Bi_5AgNb_4O_{18}$ were found to be $R_{wp} = 0.0507$ and $R_p = 0.0430$ for 3099 observed data. The goodness of fit (χ^2) value was determined to be 1.144 with 88 variables. The well-behaved anisotropic thermal parameters of the atoms suggested a correct model for the structure. Fig. 2 illustrates the Rietveld refinement results for $Bi_5AgNb_4O_{18}$. In this diagram, the upper graph shows the fit between the experimental and calculated patterns, while the lower graph shows the difference between these two patterns.

Table 1a gives the atomic coordinates, isotropic displacement factors, and site symmetry of the cations, and Table 1b gives the anisotropic displacement factors. The refinement results show that all oxygen sites are fully occupied. Ag was found to substitute only on site Bi1 with an occupancy of 0.50(3), giving rise to the unit-cell content of $Bi_{10}Ag_2Nb_8O_{36}$, or the chemical formula of $Bi_5AgNb_4O_{18}$, with $Z = 2$. The site occupancy of Bi and Ag was refined to be $\frac{1}{2}$ and $\frac{1}{2}$. The reference pattern for $Bi_5AgNb_4O_{18}$ is listed in Table 2 and has been submitted to the PDF.

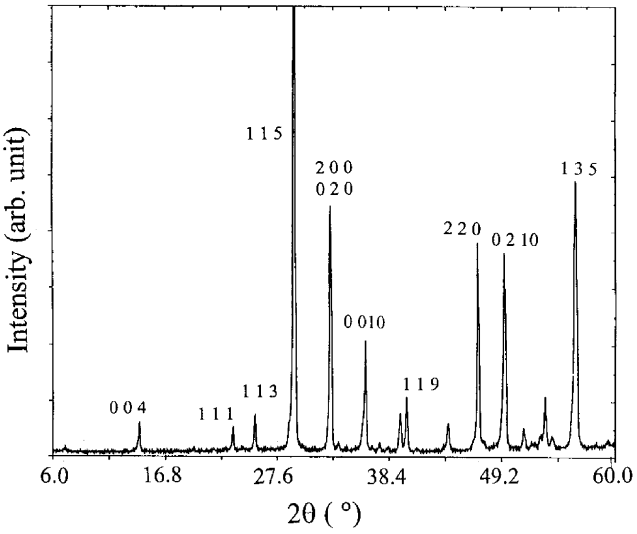

Fig. 1. X-ray powder diffraction pattern for $Bi_5AgNb_4O_{18}$.

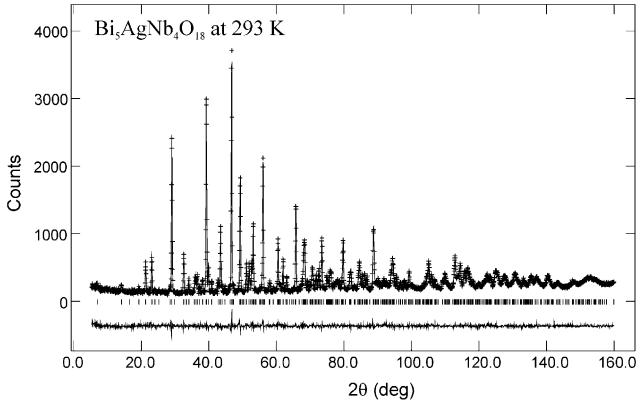

Fig. 2. Rietveld refinement results for $Bi_5AgNb_4O_{18}$. The upper graph shows the fit between the experimental and calculated patterns, while the lower graph shows the difference between these two patterns.

Selected area electron diffraction (SAD) patterns from the $Bi_5AgNb_4O_{18}$ were consistent with the lack of long-range cation ordering in the mixed Bi/Ag planes, as no multiplication of either a- or b-lattice parameters was observed (Fig. 3). However, weak diffuse reflections (indicated by arrows in Fig. 3) violate $h\,k\,0 : k = 2n$ reflection conditions for the $A2_1ma$ space group. Formally, these reflections can be accounted for by double diffraction on the $k = [021]^*$ reflections (indicated as I and II in Fig. 3) of the twin-related variants of the $A2_1ma$ structure having mutually perpendicular a- and b-axis. Yet, the diffuse nature of these reflections (all other reflections appear sharp) suggest that they either originate from scattering in the high-order Laue zones or from local reductions in symmetry associated with ion displacements (e.g., oxygen). Unfortunately, poor quality of the TEM specimens precluded detailed analyses of a single crystallographic variant which was necessary to resolve the ambiguity.

3.2. Structural description of $Bi_5AgNb_4O_{18}$

The structure of $Bi_5AgNb_4O_{18}$ belongs to the $m = 2$ member of the family of the Aurivillius phases, $(Bi_2O_2)^{2+}$ $(A_{m-1}Nb_mO_{3m+1})^{2-}$, and A =(Ag, Nb), which is characterized by perovskite-like $(A_{m-1}B_mO_{3m+1})^{2-}$ slabs regularly interleaved with $(Bi_2O_2)^{2+}$ layers. The first 14 members of the Aurivillius phase family were discovered by Aurivillius between 1949 and 1952 [16–19]. Detailed information about other $m = 2$ Aurivillius family compounds have also been reported in the literature. For example, in addition to the $Bi_5NaNb_4O_{18}$ and $Bi_5KNb_4O_{18}$ compounds [14], the crystal chemistry and crystallography of the $Bi_2ANb_2O_9$ (A =Ba, Sr, Ca, Pb) [20–23] and $Bi_2ATa_2O_9$ (A =Ba, Sr, Ca, Pb) [24–27] series are also available. Furthermore, Boullay et al. [28] proposed a generalized structural model of the Aurivillius-type compounds using a 4D superspace group

Table 1
(a) Structural parameters, site symmetry, and isotropic equivalent displacement factors for $Bi_5AgNb_4O_{18}$ at 293 K[a] and (b) anisotropic displacement parameters $U_{ij} \times 100$ (Å^2) for $Bi_5AgNb_4O_{18}$ at 295 K

Atom	Site	x	y	z	$U_{eqiv} \times 100$ (Å^2)	
(a)						
Bi(1)/Ag	4*a*	0.0128(10)	0.7550(9)	1/2	1.98	
Bi(2)	8*b*	0[b]	0.7289(5)	0.69958(8)	1.77	
Nb	8*b*	0.0401(9)	0.2493(8)	0.58529(8)	0.89	
O(1)	4*a*	0.0780(15)	0.1897(12)	1/2	2.21	
(2)	8*b*	0.0611(12)	0.3024(8)	0.65867(12)	2.52	
O(3)	8*b*	0.2744(13)	0.5076(8)	0.24983(17)	1.26	
O(4)	8*b*	0.2757(12)	0.5345(8)	0.56990(15)	1.74	
O(5)	8*b*	0.3578(10)	0.0497(9)	0.58718(18)	1.87	
	U_{11}	U_{22}	U_{33}	U_{12}	U_{13}	U_{23}
(b)						
Bi(1)/Ag	2.50(32)	2.06(26)	1.39(17)	−1.41(25)	0	0
Bi(2)	1.77(21)	1.45(15)	2.08(10)	0.18(14)	0.86(13)	0.62(12)
Nb	1.05(16)	0.52(15)	1.10(9)	−0.14(16)	−0.30(16)	−0.17(14)
O(1)	3.86(48)	2.21(43)	0.56(22)	−0.32(24)	0	0
O(2)	3.97(35)	3.13(34)	0.47(15)	−0.48(24)	0.42(24)	−0.69(18)
O(3)	1.69(20)	0.85(17)	1.24(10)	−0.01(24)	0.21(21)	0.39(23)
O(4)	0.69(16)	1.52(25)	3.01(19)	−1.29(22)	−0.78(21)	0.34(20)
O(5)	1.82(19)	1.05(26)	2.74(23)	0.26(15)	−0.10(20)	−0.11(21)

$R_p = 4.3\%$, $R_{wp} = 5.07$, $\chi^2 = 1.144$.
[a] Space group $A2_1am$ (#36), $a = 5.49153(18)$ Å, $b = 5.47518(17)$ Å, $c = 24.9282(8)$ Å, and $V = 749.52(4)$ Å^3, $Z = 2$. The site occupancy is 1.0 for all atoms, except for Bi1 [0.50(3)]/Ag [0.50(3)].
[b] Fixed at 0 to fix the origin along the *a* axis.

analysis where the structures are considered as cation-deficient perovskites with the general formula $AB_{1-x}O_3$.

The prototype structure of the Aurivillius family of compounds has the $I4/mmm$ tetragonal symmetry. In the $I4/mmm$ structure, the Bi atoms adopt a square pyramid coordination. The *A*-sites are surrounded by 12 oxygen atoms in an icosahedral coordination, while the *B*-sites are six-fold coordinated by oxygen. Fig. 4 reproduces the layered structure of $Bi_5AgNb_4O_{18}$. The Bi_2O_2 (site Bi2) layers contain no Ag. Disordered Ag and Bi1 were found only in the layers between the two distorted [NbO_6] octahedra along the *c*-axis. Table 3a summarizes selected bond distances in the Bi1/Ag–O, Bi2–O, and Nb–O polyhedra.

The bond valence sum (BVS) for Bi, Ag, and Nb were calculated using equations derived by Brown and Altermatt [29,30]. The atomic valence V_i of an atom *i* is defined as the sum of the bond valences v_{ij} of all the bonds from atom *i* to atoms *j*:

$$\sum_j v_{ij} = V_i.$$

The most commonly adopted empirical expression for the bond valence v_{ij} as a function of the interatomic distance d_{ij} is

$$v_{ij} = \exp\left[(r_0 - d_{ij})/B\right].$$

The parameter *B* is commonly taken to be a "universal" constant equal to 0.37 Å. Values of the reference distance r_0 are tabulated for various pairs of atoms [30]. The bond valence calculation can be used as a semi-quantitative method to estimate local residual strain. For example, a BVS value greater than an expected value will indicate an overbonding ("crowded") situation, or the site is under compressive stress. Results of bond valence calculations for $Bi_5AgNb_4O_{18}$ are shown in Table 3a. The r_0 values used are 1.911 Å for Nb–O, 2.118 Å for Sr–O, and 1.920 Å for Ta–O. The BVS value for Bi1 is computed using the bond valence values of both Bi–O and Ag–O weighted by the site occupancy.

3.2.1. Bi–O polyhedra

The $6s^2$ lone-pair electrons of Bi^{3+} influence significantly a distortion of the coordination environment around the Bi ions. Both Bi1 and Bi2 adopt highly anisotropic environments. Among the 12 Bi1/Ag–O distances that were listed in Table 3a, four are greater than 3.0 Å. Therefore, the Bi1 coordination is best described as eight-fold, according to the sum of effective ionic radii [14,31,32]. Since Bi2 is not 12-fold coordinated, its coordination environment is different from that in the prototype $I4/mmm$; note that four out of 10 Bi2–O distances are greater than 3.0 Å. The distortion of both Bi1 and Bi2 coordination environments can be estimated from the distortion ratio values (the ratio of the shortest to the longest bond distance, with '1' being undistorted). The values of 0.772 and 0.637 for Bi1/Ag,

Table 2
X-ray powder diffraction pattern for $Bi_5AgNb_4O_{18}$, space group $A2_1ma$ ($a=5.4915(2)$ Å, $b=5.4752(2)$ Å, $c=24.9282(8)$ Å, and $V=749.52(4)$ Å^3, $Z=2$)

d (Å)	I	h	k	l	d (Å)	I	h	k	l	d (Å)	I	h	k	l
12.4643	29	0	0	2	6.23214	90	0	0	4	4.57158	6	0	1	3
3.83093	36	1	1	1	3.68617	5	0	1	5	3.51338	56	1	1	3
3.11697	38	0	0	8	3.06054	999*	1	1	5	2.98520	11	0	1	7
2.74561	174	2	0	0	2.73729	182	0	2	0	2.68133	6	2	0	2
2.62270	6	1	1	7	2.51259	16	2	0	4	2.50620	13	0	2	4
2.49285	112	0	0	10	2.40380	7	1	2	2	2.29063	20	2	0	6
2.28579	19	0	2	6	2.25376	56	1	1	9	2.06003	14	2	0	8
2.05651	15	0	2	8	1.95650	6	1	1	11	1.93849	182	2	2	0
1.91546	9	2	2	2	1.85102	22	2	2	4	1.84562	110	2	0	10
1.84308	108	0	2	10	1.78125	25	0	3	3M	1.78125	25	0	0	14M
1.75669	7	2	2	6	1.74729	5	1	2	10	1.73176	13	3	1	1
1.71883	43	1	1	13	1.69926	11	3	1	3	1.69531	8	1	3	3
1.64598	15	2	2	8	1.63942	144	3	1	5	1.63587	149	1	3	5
1.58441	10	1	2	12	1.56043	8	3	1	7	1.53027	93	2	2	10
1.52748	86	1	1	15	1.49423	18	2	3	3M	1.49423	18	2	0	14M
1.49260	13	0	2	14	1.47094	13	3	1	9	1.46837	11	1	3	9
1.38492	5	0	0	18	1.37281	19	4	0	0	1.36864	21	0	4	0
1.31135	15	2	2	14	1.28694	11	3	1	13	1.28522	13	1	3	13
1.25099	49	3	3	5	1.24643	7	0	0	20	1.24279	17	1	1	19
1.23614	10	2	0	18M	1.23614	10	0	2	18M	1.22713	22	4	2	0
1.22489	22	2	4	0	1.20252	17	4	0	10	1.19977	78	1	3	15+
1.17113	5	3	3	9	1.13465	20	2	0	20M	1.13465	20	0	2	20M
1.12688	10	2	2	18	1.10097	30	4	2	10	1.09935	27	2	4	10
1.07167	5	3	3	13	1.05252	23	5	1	5	1.04971	25	1	5	5
1.04841	15	2	2	20	1.04670	9	3	1	19	1.04578	9	1	3	19
1.04383	7	1	1	23	1.02018	15	3	3	15	1.01042	6	4	2	14
1.00917	6	2	4	14	0.97130	10	2	0	24M	0.97130	10	0	2	24M
0.96925	10	4	4	0	0.96571	7	1	1	25	0.92465	19	5	3	5
0.92325	26	3	5	5M	0.92325	26	4	0	20M	0.92154	5	0	4	20
0.92070	7	3	3	19	0.91937	6	3	1	23	0.91874	7	1	3	23
0.91554	12	2	2	24	0.90352	32	5	1	15M	0.90352	32	4	4	10M
0.90190	13	1	5	15	0.87445	14	4	2	20	0.87364	10	2	4	20
0.86797	10	6	2	0	0.86587	11	2	6	0	0.86446	16	3	1	25M
0.86446	16	1	3	25M	0.85922	15	2	2	26M	0.85922	15	6	0	10M
0.85684	10	0	6	10	0.85130	6	4	4	14	0.84963	5	6	2	6
0.83922	17	1	1	29	0.83236	9	5	1	19	0.83096	12	1	5	19
0.83045	7	3	3	23	0.82831	7	4	0	24	0.82740	8	0	4	24

Symbol 'd' refers to d-spacing values, 'I' refers to integrated intensity value (scaled according to the maximum value of 999; the symbol (*) indicates the strongest peak), the $h\,k\,l$ values are the Miller indexes, M and+ refer to peaks containing contributions from two and more than two reflections, respectively. The intensity values reported are integrated intensities rather than peak heights.

Bi2, respectively, are substantially lower than unity. For the Bi1 site, which is filled by 50%/50% mixture of Bi and Ag, the Bi1/Ag–O bonds range from 2.407(8) to 2.691(6) Å (considering an eight-fold coordination). Fig. 5 shows the highly distorted coordination environment around the Bi2. The relatively large distances between Bi2 and O2, O5, and O5′ of the [NbO_6] unit (3.32, 3.85, and 3.1 Å, respectively) suggest that the $6s^2$ lone-pair electrons are likely to be located in this region.

The BVS of 1.86 for the Bi1/Ag-site compares well with the expected value [BVS] of 2.0. This value would have been much greater, 2.548, if only Bi was assumed to be the sole occupant. The value of 2.548 is much smaller than the ideal BVS value for Bi^{3+} of 3, indicating if only Bi occupies the site, tensile stress due to underbonding will result (or the cage in which Bi1 is located would be 'too large'). Apparently, the larger size Ag^{1+} substitution stabilizes the Bi1-site by reducing the tensile stress.

The Bi2 atoms in the $(Bi_2O_2)^{2+}$ layers do not exhibit the four-fold coordination as that found in the $I4/mmm$ prototype structure [14]. Because of the tilting of the NbO_6 octahedra in the perovskite layers (discussed below), in addition to the four bonds that form the square pyramidal geometry (an average Bi–O distance of 2.315 Å), two longer Bi2–O bonds were also found to connect to the apex O2 (2.570(5) and 2.623(6) Å). The remaining Bi2–O distances (3.318(5), 3.250(6), 3.572(4), and 3.151(5) Å) listed in Table 3a can be considered as non-bonding [14]. The BVS value for Bi2 (2.927) is not significantly different from the ideal value of 3.00.

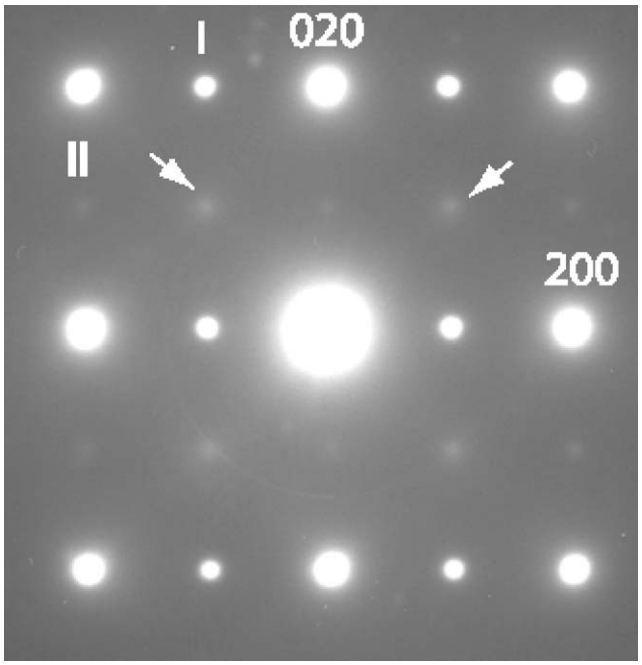

Fig. 3. SAD patterns of $Bi_5AgNb_4O_{18}$. No multiplication of either *b*- or *c*-lattice parameters was observed. Weak diffuse reflections are indicated by arrows.

3.2.2. *[NbO_6] octahedra*

Nb was found to have a distorted octahedral environment (Fig. 6). The mean Nb–O distance, 1.996 Å, is close to the sum of the effective ionic radii, 2.04 Å [31,32]. Table 3b gives the bond angles for the [NbO_6] octahedron. The Nb–O distances range from 1.856(4) to 2.161(2) Å and the O–Nb–O angles range from 81.99(24)° to 98.52(27)°. The distortion ratio for [NbO_6] was determined to be 0.859. The BVS value for Nb (4.971) is very close to the ideal value of 5, which indicates lack of substantial residual strain around Nb.

The perovskite-like slabs in the $Bi_5AgNb_4O_{18}$ structure feature tilting of [NbO_6] octahedra which relieves tensile bond strain about both Bi1/Ag- and Bi2-cation sites (Fig. 6). This tilting can be described as a combination of rotations about both *a*- (rotation angle 10.3°) and *c*-axis (rotation angle 12.4°) of the orthorhombic structure. The octahedra in both layers of the slab feature in-phase tilting about the pseudo-tetragonal *c*-axis (parallel to the four-fold symmetry axes of octahedra). The sign of rotation about the *a*-axis (parallel to the two-fold symmetry axes of the octahedra) is constrained, so that the adjacent octahedra rotate in opposite directions. The tilting pattern in the perovskite-like slabs of the $Bi_5AgNb_4O_{18}$ structure corresponds to the $b^-\,b^-\,c^+$ Glazer's tilt system [33] (note, that '*b*' and '*c*' letters in this notation correspond to the [110] and [001] directions of the $Bi_5AgNb_4O_{18}$ structure, respectively).

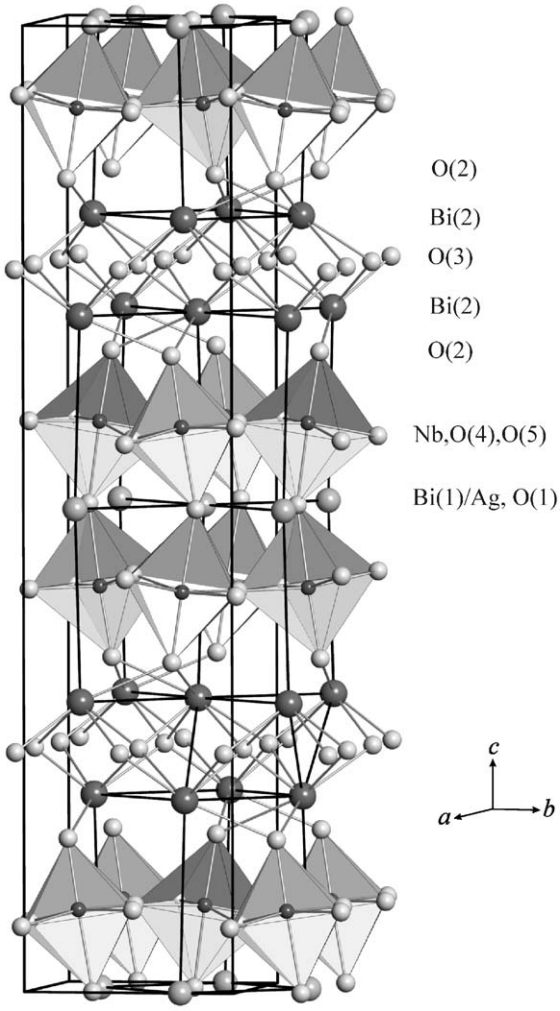

Fig. 4. Structure of the Aurivillius phase, $Bi_5AgNb_4O_{18}$ showing the perovskite-like $(Bi_{m-1}(Bi,\ Ag)_mO_{3m+1})^{2-}$ slabs regularly interleaved with $(Bi_2O_2)^{2+}$ layers. Ag was found to substitute at the Bi2-site.

3.3. *Comparison of the $(Bi_2O_2)^{2+}$ $(A_{m-1}Nb_mO_{3m+1})^{2-}$ (A = Na, Ag, and K; m=2) structures*

In these three compounds, all Bi-, Bi/Ag-, and Nb-sites have a distorted environment relative to the prototype structure [14]. A comparison of the orthorhombic distortion of the unit-cell parameters (Table 4) indicate that there is a trend correlated with the size of the *A*-cation. The magnitude of orthorhombic distortion occurs in the order of $A = K < Ag < Na$. The Shannon ionic radius for Na^{1+}, Ag^{1+}, and K^{1+}, using the VIII coordination data, are 1.18 Å, 1.28 Å, and 1.51 Å, respectively [31,32]. Therefore, a general trend is that the distortion of the structure decreases with the increasing size of the '*A*'-cation in $(Bi_2O_2)^{2+}(A_{m-1}B_mO_{3m+1})^{2-}$. It is plausible that the distortion of the Bi–O, Bi/A–O polyhedra, and the rotation angles of the NbO_6 octahedra with respect to the *a* and *c*-axis both contribute to the orthorhombic

Table 3
(a) Selected bond lengths in tetragonal $Bi_5AgNb_4O_{18}$[a] and (b) bond angles of the NbO_6 octahedron (°)

M–O	Distances (Å)	Ave. distance (Å)	Distortion ratio	BVS
(a)				
(1) Bi1/Ag–O1	3.116(8)	2.775	0.772	1.88/[2.0][b]
	2.407(8) × 2			1.74[c]
	3.119(9)			
Bi1/Ag–O4	2.565(7) × 2			
	2.691(6) × 2			
Bi1/Ag–O5	3.304(6) × 2			
	2.567(6) × 2			
(2) Bi2–O2	2.570(5)	2.686	0.637	2.96
	3.318(5)			
	2.623(6)			
	3.250(6)			
	3.572(4)			
Bi2–O3	2.191(5)			
	2.309(6)			
	2.484(6)			
	2.277(6)			
Bi2–O5	3.151(5)			
(3) Nb–O1	2.161(2)	1.996	0.859	4.971
Nb–O2	1.856(4)			
Nb–O4	2.064(6)			
	1.913(6)			
Nb–O5	2.059(6)			
	1.920(7)			
(b)				
O(1)–Nb–O(2)	170.9(4)			
O(1)–Nb–O(4)	82.58(27)			
O(1)–Nb–O(4)	88.24(22)			
O(1)–Nb–O(5)	81.99(24)			
O(1)–Nb–O(5)	86.88(30)			
O(2)–Nb–O(4)	91.48(25)			
O(2)–Nb–O(4)	98.52(27)			
O(2)–Nb–O(5)	90.45(29)			
O(2)–Nb–O(5)	98.16(24)			
O(4)–Nb–O(4)	88.30(18)			
O(4)–Nb–O(5)	82.80(29)			
O(4)–Nb–O(5)	167.63(27)			
O(4)–Nb–O(5)	167.54(26)			
O(4)–Nb–O(5)	97.86(32)			
O(5)–Nb–O(5)	89.35(18)			

[a] Distances printed are those <3.6 Å. BVS is the bond valence calculated from the measured bond distances and from reference values given by Brese and O'Keeffe [29] and Brown and Altermatt [30] (2.094 Å for Bi–O, 1.911 Å for Nb–O, and 1.805 Å for Ag–O). [BVS] is the expected valence value weighted by site occupancy.

[b] BVS value for the Bi1-site is computed using the bond valence value of Bi–O and Ag–O weighted by the site occupancy.

[c] Empirical constants from Brown and Altermatt [29]: $B = 0.37$; r_0 (Bi/Ag) = $(r_0(\mathrm{Bi}) + r_0(\mathrm{Ag}))/2$.

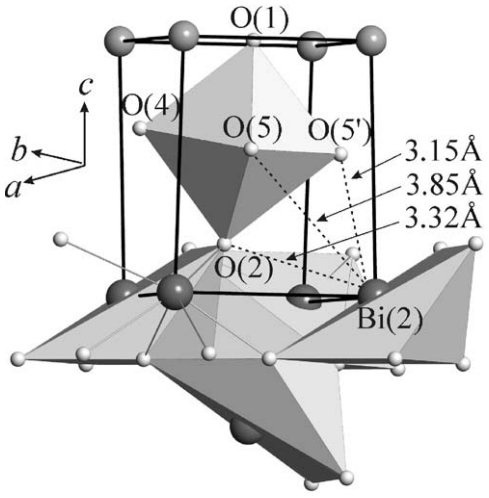

Fig. 5. Distorted environment around Bi(2) showing the relatively large distances from Bi2 to O(2) and O(5) of the NbO_6 unit. This is the region where the Bi $6s^2$ lone-pair electron is likely to be located.

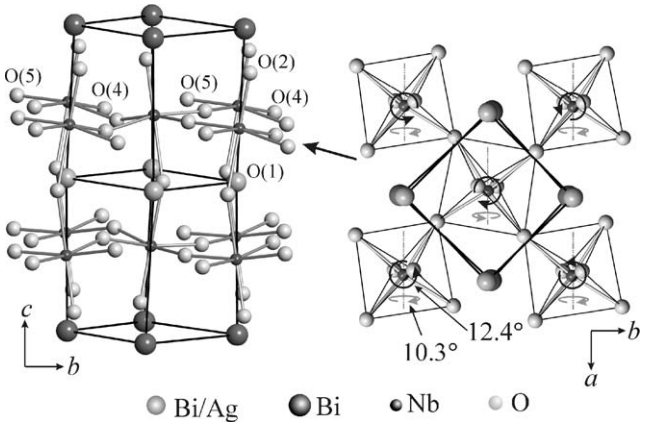

Fig. 6. Distorted NbO_6 perovskite layer showing rotation angles around *a*- and *c*-axis in $Bi_5AgNb_4O_{18}$.

Table 4
Lattice parameters for $Bi_5MNb_4O_{18}$, M = Na, Ag, and K

	M = Na	M = Ag	M = K
a (Å)	5.4937(3)	5.4915(2)	5.5005(8)
b (Å)	5.4571(4)	5.4752(2)	5.4958(8)
c (Å)	24.9169(14)	24.9282(8)	25.2524(16)
V (Å^3)	747.00(8)	749.52(4)	763.37(17)

The orthorhombic distortion is the smallest for M = K, followed by M = Ag. The largest distortion is found in M = Na.

distortion, which increases progressively in the K→Ag→Na sequence. Suárez et al. [34] reported that the distortion of the Aurivillius compounds are related to the perovskite tolerance factor, t, where $t = (R_A + R_O)/\sqrt{2}(R_B + R_O)$ (R_A, R_B, and R_O are the average effective ionic radii of the *A*- and *B*-cations and oxygen in the Aurivillius formula unit, $(Bi_2O_2)^{2+}(A_{m-1}B_mO_{3m+1})^{2-}$). The t values for these three $(Bi_2O_2)^{2+}(A_{m-1}Nb_mO_{3m+1})^{2-}$ analogs are 0.919, 0.896, and 0.791 for A =K, Ag, and Na, respectively. Our observation agrees with that reported by Suárez

Table 5
BVS values for the Bi1/A-, Bi2-, and Nb-sites in the $(Bi_2O_2)^{2+}$ $(A_{m-1}Nb_mO3_{m+1})^{2-}$ compounds (A = Na, Ag, K)

	Bi1/A	Bi2	Nb
Na	1.99	2.99	4.92
Ag	1.74 (1.88)	2.96	4.97
K	2.63	2.83	4.97

BVS values for both Na- and K-based compounds were taken from Ref. [14]. Values for the Ag-compound is taken from Table 4.

et al. [34] in that as t decreases the structural distortion increases.

The [NbO_6] octahedral rotations around the a-axis for the three compounds all have similar values. The tilting angles about this axis are 10.3°, 10.3°, and 7.2° for A =Na, Ag and K, respectively. The corresponding tilting angles around the c-axis are 9.4°, 12.4°, and 7.2°, respectively. While these values are close to each other, they do not seem to follow a trend, possibly because of different electronic properties in that Ag^{1+} is a transition element, while both K and Na are alkali metals without d-orbitals.

The BVS values for the Bi1/A-, Bi2-, and Nb-sites in the three $(Bi_2O_2)^{2+}$ $(A_{m-1}Nb_mO3_{m+1})^{2-}$ compounds (A =Na, Ag, and K) are summarized in Table 5. According to these results, the tensile bond strain about the Bi2-sites increases monotonically on going from Na to K. At the same time, the small residual tension around the Nb-site, as observed for the Na-based compound, is reduced to near zero for both Ag- and K-based analogs. In contrast, no such clear trend is observed for the mixed Bi1/A-sites.

The Bi2–O2 axial bond distances (2.550(6) Å, 2.622(11) Å for A =Na; 2.570(5) Å, 2.623(6) Å for A =Ag; and 2.73(2) Å, 2.772(11) Å for A =K) also exhibit a clear trend. These distances are significantly longer than the four bonds that form the distorted square pyramid. The distorted geometry is most likely due to the presence of the Bi $6s^2$ lone-pair electrons.

4. Summary

The structure of the $m = 2$ Aurivillius phase, $Bi_5AgNb_4O_{18}$, was refined by the powder neutron Rietveld technique. The $6s^2$ lone-pair electrons of Bi give rise to the distorted environment of both Bi1 and Bi2. Results of bond valence calculations show that the substitution of the larger Ag^{1+} is into the Bi1-site stabilizes this site by reducing the tensile bond strain around the Bi1. $Bi_5AgNb_4O_{18}$ was found to be isostructural to $Bi_5NaNb_4O_{18}$ and $Bi_5KNb_4O_{18}$ [14]. A comparison of the rotation angles of the NbO_6 octahedra in these three analogs with respect to the a- and c-axis indicates that these rotations are affecting the orthorhombic distortion of the unit cell, which increases progressively in the K → Ag → Na sequence (illustrated in the orthorhombic distortion of unit cell-parameters). The structural distortion of these compounds increases with decreasing perovskite tolerance factor.

Acknowledgments

The authors acknowledge the partial support from the MSEL Director's Reserve Fund. Nils Swanson is thanked for his graphical assistance.

References

[1] R.R. Tummala, J. Am. Ceram. Soc. 74 (5) (1991) 895–908.
[2] Multilayer LTCC Modules, Microwave J. 44 (2) (2001) 182.
[3] A low-loss, lead-free LTCC system for wireless and RF applications, Microwave J. 41 (12) (1998) 104.
[4] M. Lanagan, Center for Dielectric Studies, Pennsylvania State University, April 17, 2001, personal communication.
[5] Seo-Yong Cho, Hyuk-Joon Youn, Dong-Wan Kim, Tae-Gyum Kim, Kug Sun Hong, J. Am. Ceram. Soc. 81 (11) (1998) 3038–3040.
[6] M. Valant, D. Suvorov, J. Am. Ceram. Soc. 83 (11) (2000) 2721–2729.
[7] R.S. Roth, J.L. Waring, J. Res. Natl. Bur. Stand. 66A (6) (1962) 451–463.
[8] E.M. Levin, R.S. Roth, J. Res. Natl. Bur. Stand. Sect. A 68 (2) (1964) 197–206.
[9] L.P. Cook, W. Wong-Ng, P. Schenck, M. Vaudin, J. Suh, IMAP Interconnect Science and Technology Symposium Proceedings, 2003.
[10] H.M. Rietveld, J. Appl. Crystallogr. 2 (1969) 65–71.
[11] A.C. Larson, R.B. von Dreele, GSAS—General Structure Analysis System, US Government contract (W-7405-ENG-36) by the Los Alamos National Laboratory, which is operated by the University of California for the US Department of Energy, 1992.
[12] R.A. Young, The Rietveld Method, International Union of Crystallography Monograph, Oxford Scientific Publications, London, 1995.
[13] J.G. Thompson, A.D. Rae, R.L. Withers, D.C. Craig, Acta Crystallogr. B 47 (1991) 174–180.
[14] S. Borg, G. Svensson, J. Solid State Chem. 157 (2001) 160–165.
[15] J.S. Kisper, K. Lonsdale (Eds.), International Tables for X-ray Crystallography II, published for the International Union of Crystallography, Reidel Publishing Co., Holland, 1985, pp. 295–298.
[16] B.J. Ismunandar, Kennedy, J. Solid State Chem. 126 (1996) 135–141.
[17] S.M. Blake, M.J. Falconer, M. McCreedy, P. Lightfoot, J. Mater. Chem. 7 (8) (1997) 1609–1613.
[18] A. Snedden, C.H. Hervoches, P. Lightfool, Phy. Rev. B 67 (2003) 92102.
[19] V. Sirkanth, H. Idink, W.B. White, E.C. Subbarao, H. Rajagopal, A. Sequeira, Acta Crystallogr. B 52 (1996) 432–439.
[20] Y. Shimakawa, Y. Kubo, Y. Nakagawa, T. Kamiyama, H. Asano, F. Izumi, Appl. Phys. Lett. 74 (13) (1999) 1904–1906.
[21] Y. Shimakawa, Y. Kubo, Y. Nakagawa, S. Goto, T. Kamiyama, H. Asano, F. Izumi, Phys. Rev. B 61 (10) (2000) 6559–6564.

[22] R. Macquart, B.J. Kennedy, B.A. Hunter, C.J. Howard, J. Phys.: Condens. Matter 14 (2002) 7955–7962.
[23] C.H. Lu, B.K. Fang, J. Mater. Res. 13 (8) (1998) 2262–2268.
[24] B. Aurivillius, Ark. Kemi. 1 (54) (1949) 463–480.
[25] B. Aurivillius, Ark. Kemi. 1 (58) (1949) 499–512.
[26] B. Aurivillius, Ark. Kemi. 2 (37) (1950) 519–527.
[27] B. Aurivillius, Ark. Kemi. 5 (4) (1952) 39–47.
[28] Ph. Boullay, G. Trolliard, D. Mercurio, J.M. Perez-Mato, L. Elcoro, J. Solid State Chem. 164 (2) (2002) 252–260.
[29] N.E. Brese, M. O'Keeffe, Acta Crystallogr. B 47 (1991) 192–197.
[30] I.D. Brown, D. Altermatt, Acta Crystallogr. B 41 (1985) 244–247.
[31] R.D. Shannon, C.T. Prewitt, Acta Crystallogr. B 25 (1969) 925–946.
[32] R.D. Shannon, Acta Crystallogr. A 32 (1976) 751–767.
[33] A.M. Glazer, Acta Crystallogr. B 28 (1972) 3384–4492.
[34] D.Y. Suárez, I.M. Reaney, W.E. Lee, J. Mater. Res. 16 (11) (2001) 3139–3149.